ISSN 0001-4338, Izvestiya, Atmospheric and Oceanic Physics, 2009, Vol. 45, No. 4, pp. 495–502. © Pleiades Publishing, Ltd., 2009.
Original Russian Text © V.E. Prokhorov, Yu.D. Chashechkin, 2009, published in Izvestiya AN. Fizika Atmosfery i Okeana, 2009, Vol. 45, No. 4, pp. 531–538.

Modeling the Generation and Gravity–Capillary Waves using an Underwater Sound Source

V. E. Prokhorov and Yu. D. Chashechkin

Institute for Problems in Mechanics, Russian Academy of Sciences, pr. Vernadskogo 101/1, Moscow, 119526 Russia
e-mail: prokhorov@ipmnet.ru

Received April 16, 2008; in final form, July 23, 2008

Abstract—This is an experimental study of the acoustic method of surface-wave excitation using an underwater source of high-frequency (950 kHz) sound. The surface waves are excited at the sound-beam modulation frequency (3–55 Hz). For a normal fall onto the free surface, the modulated sound beam efficiently generates waves in the gravity–capillary range. This provides flexible electronic control of the main wave parameters (frequency and amplitude) in the packet and continuous modes. The amplitude–frequency characteristics of the process of surface-wave generation were obtained by numerical calculations (based on equations for the rate of acoustic flux and propagation of gravity–capillary surface waves) and by experiments (based on surface wave measurements by optical and contact methods). Both values are very consistent: on the background of a similar monotonic attenuation with frequency, they have a local dip near the minimum of the phase velocity and oscillation in the frequency range above 20 Hz. The experiments on the excitation of wave packets by single acoustic messages with varying lengths and powers, as well as by falling water drops, indicated that, in all cases, the phase characteristics are satisfactorily consistent with one another and the time needed for the signal to arrive at the measurement point is determined by the group velocity.

DOI: 10.1134/S0001433809040094

INTRODUCTION

In recent years the traditional interest in the study of surface surface wave has increased due to the search for conditions of anomalous amplitude wave generation, which is highly dangerous to coastal buildings and ships [1]. One fast-evolving method of sea-surface wave parameters is remote sensing, which makes it possible to determine the surface and underwater parameters [2]. A sounding procedure normally uses radio waves in the centimeter and millimeter ranges, with their length being comparable with that of gravity–capillary waves. The properties of short surface waves, which depend on many factors, have been actively investigated theoretically and experimentally in the field and in laboratory conditions [2, 3].

The theoretical investigations are directed mainly at describing steady-state surface surface wave [4, 5], analyzing dissipation and nonlinearity effects [6, 7], and refining dispersion relations [8]. In laboratory investigations, the gravity–capillary waves are usually generated by mechanical wave producers [9, 10] with restricted functional capabilities. One alternative way to create waves is using the radiative effect of underwater sound on the surface, which makes it possible to create a controllable surface relief with a given temporal variability of the rise form and amplitude [3]. The varying relief area serves as a source of surface waves, which, unlike mechanical wave producers, generates no additional perturbations of either a wave or non-wave character (vortices or boundary layers). This paper investigates dispersion and the phase properties of ring gravity–capillary surface waves created by a disk underwater acoustic resonator.

EXPERIMENTAL TECHNIQUE

A schematic of the experimental installation is shown in Fig. 1. The experiments were performed in a tank (*1*) of dimensions $145 \times 50 \times 60$ cm^3 filled with degassed tap water. The tank has a disk resonator (*2*) of diameter 2.5 cm made of TsTS-19 piezoceramic with a mechanical resonance frequency of 950 kHz. This resonator is supplied by amplitude-modulated signal with a controlled frequency and modulation rate from a generator (*3*) through a power amplifier (*4*). The form of the modulated signal is determined by the conditions of a particular experiment. An emitted axisymmetric acoustic beam (*5*) is directed vertically upward and generates a pulsed elevation of the free surface, which is the source of propagating ring waves. The typical width of the contact patch between the beam and free surface (which determines the size of the wave-generation area) is 3 cm.

The tank has an electromechanical wave producer (*6*) with a driving generator (*7*), making it possible to produce plane surface waves. The actuating body of the wave producer is a thin vertical plate 35 cm in length with a height of 1 cm and a thickness of 0.5 mm

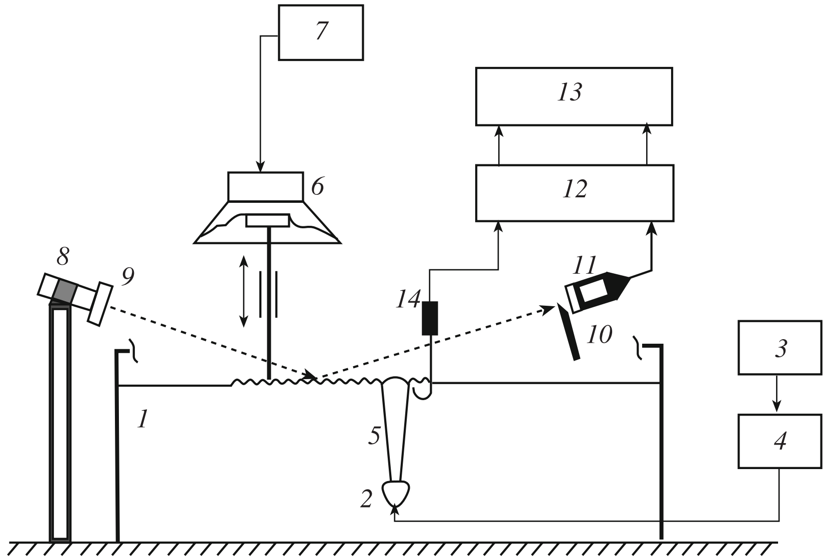

Fig. 1. Schematic of the laboratory setup: (*1*) the tank 145 × 50 × 60 cm^3, (*2*) high-frequency acoustic resonator, (*3*) driving generator, (*4*) power amplifier, (*5*) sound beam, (*6*) wave producer of surface surface wave with a generator, (*7*, *8*) laser with collimator, (*9*, *10*) diaphragm, (*11*) photo receiver, (*12*) interface, (*13*) computer, and (*14*) microcontact elevation sensor.

that varies vertically in amplitude (from 0.1 to 3 mm) and in frequency (from 5 to 70 Hz).

The wave-induced slope variations and free-surface positions were registered by remote (*8–13*) and contact (*12–14*) instruments. The optical system for wave-slope measurements, which is traditionally used in laboratory experiments with surface waves [11], consists of a semiconductor laser (*8*) with a wavelength of 0.650 μm, a collimator (*9*) for ray focusing at a given surface point, a visualizing diaphragm (*10*), and a photodetector (*11*) installed on an aligning table and connected with a computer (*13*) through interface (*12*). Visualizing diaphragm (*10*) cuts a outpution of the light beam off and makes it possible to register the elevation and cavity forms.

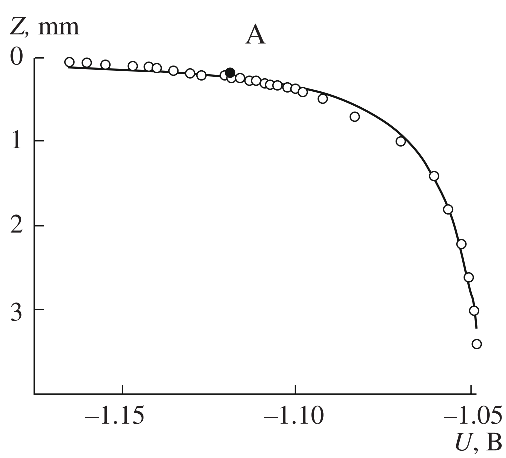

Fig. 2. Calibration curve of the contact sensor (the light circles denote experimental values, the solid line denotes the approximation by the Lorenz function). Point A denotes the sensor level.

Interface (*12*), which was specially developed for this experiment, has four independent outputs, each of which has a programmable amplifier with a coefficient from –40 to +40 dB, a 12-bit analog-to-digital converter, and a memory unit. The control circuit compresses data for all channels and transmits to the computer through a USB line. The user interface makes it possible to select the measured channels and set the sampling time, amplification coefficient, measurement delay, and sample length for each individual channel.

The sensor of contact elevation measuring unit (*14*) (the end surface of the capillary of diameter 0.8 mm, where the central platinum-wire electrode is embedded [12]) was located under water at a distance of some 0.3 mm away from the free surface. The wave oscillations led to noticeable variations in the field of electrical conduction near the sensor and to a corresponding change in the output signal. The calibration parameter approximated by the Lorenz function $z = a_0 + \frac{2a_1}{\pi}\left(\frac{a_2}{4(U-U_2)^2} + a_2^2\right)$, is shown as a solid line in Fig. 2 (the empirical constants are $a_0 = -0.012$, $a_1 = -0.98$, $a_2 = 0.011$, and $U_0 = -1.02$). It follows from the calibration parameter that the sensitivity at the working interval is 6.6 V/mm. During wave measurements, the sensor does not cross the free surface, thus essentially increasing its performance.

Prior to the start of experiments, the optical system (*8–11*) was adjusted and the contact meter was calibrated for undisturbed free surface, the acoustic and

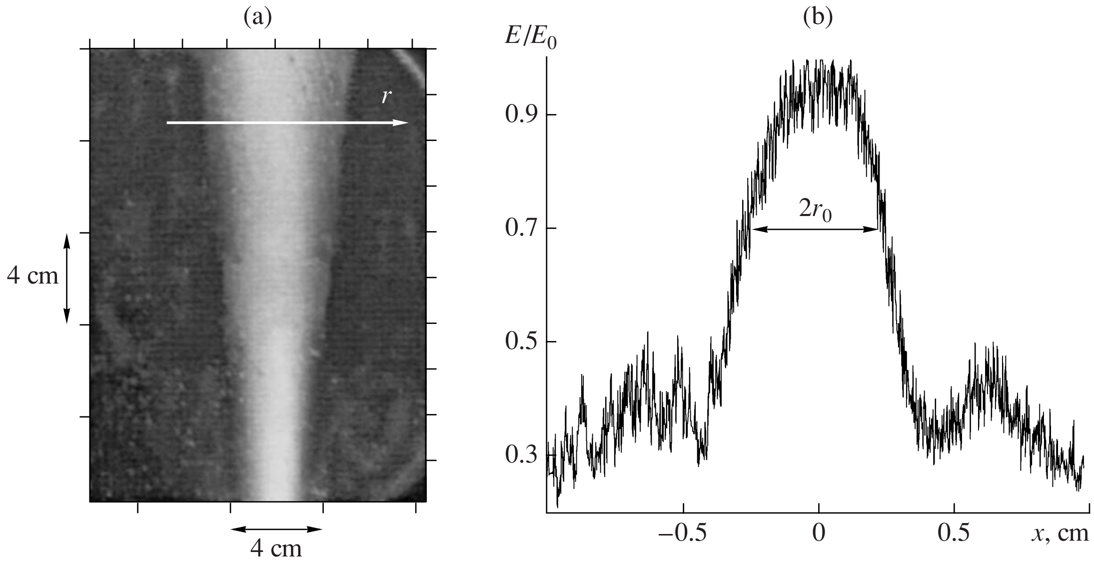

Fig. 3. Acoustic beam. (a) Shadow pattern for a three-fold nominal power, and (b) cross distribution of image illumination for a nominal power.

mechanical wave producers were tuned, and a walk-through for linear measurements was conducted.

The form of an acoustic beam is illustrated by its shadow image (Fig. 3a). To obtain a pictorial pattern, the resonator binders were supplied with increased power. In the generation mode, the power was essentially lower, the beam image was low-contrast, and the beam geometry was determined by the cross distribution of illumination E normalized to the maximum value E_0 at the beam center (Fig. 3b). It can be seen from Fig. 3b that the side lobes are weakly expressed and their contribution to the surface deformation is slight.

The wave field was registered after the termination of transient processes and the acquisition of a stationary wave pattern. A series of experiments compares the characteristics of short wave packets generated by a short-time turning on of the acoustic beam or by a fall of the water drop.

MAIN RESULTS

A typical pattern of ring gravity–capillary waves generated by an acoustic beam is shown in Fig. 4. The dark spot of radius R in the center of this figure marks the area of surface deformation by the acoustic beam. In most experiments the sound intensity was slight and the wave amplitude satisfied the requirements of linear theory [11, 12].

One objective of the experiments was to investigate the possibility of separating the wave components created by the acoustic beam in the background of plane waves from the mechanical wave producer. In these experiments the light spot of the optical system was focused on a 2 mm point of diameter which was located in the line connecting the centers of the plate and light spot. The distances from the spot to the plate and to the beam center were equal to 15 and 30 cm, respectively. Due to the great distance, the front of the wave traveling from the light source to the measurement point became more plane.

The graphs of registered signals from the output of photo receiver, which was normalized to a maximum value, illustrate the change in the form of the total surface wave when the frequencies of both wave types are increased (Fig. 5a). The ratio of the frequency of sound-beam modulation to the frequency of mechanical wave producer was equal to 0.3 for all cases. The relative contribution of each source to the total signal

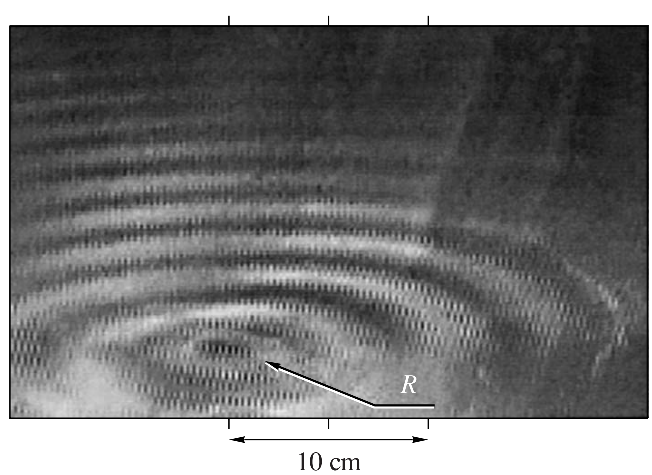

Fig. 4. Surface ring waves from the acoustic beam. The frequency of beam modulation is 6 Hz.

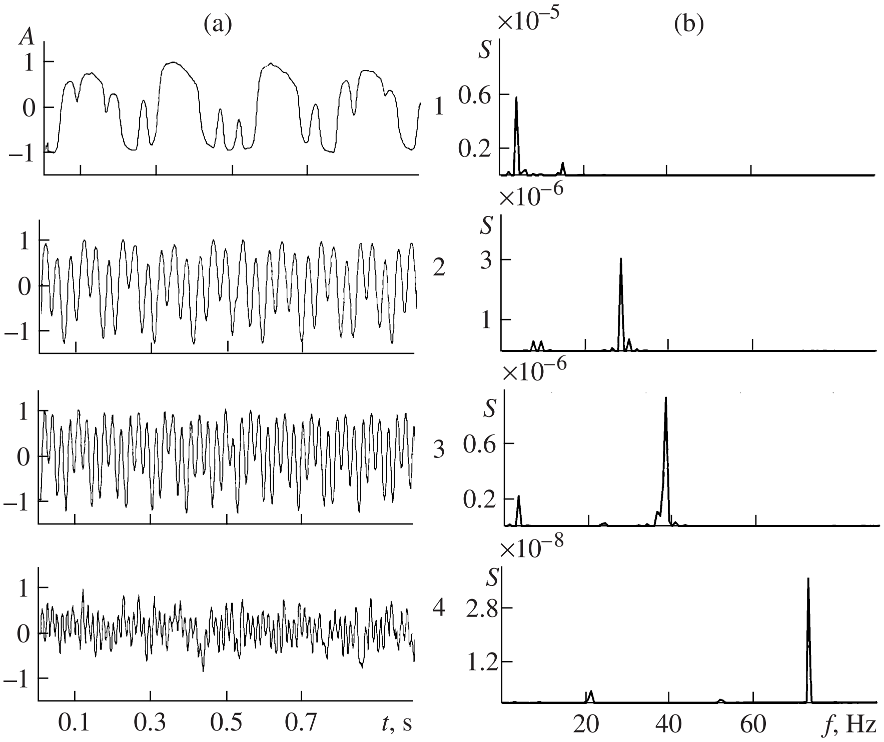

Fig. 5. Normalized (a) amplitudes and (b) spectra of surface waves from underwater acoustic and surface electromechanical wave producers. The frequencies of acoustic and surface wave producers are (in Hz): *1* – 4 and 15, *2* – 9 and 30, *3* – 45 and 13, and *4* – 23 and 75, respectively.

is illustrated by the distributions shown in Fig. 5b. In the low-frequency range, the contribution of the sound generator is dominant (Fig. 5b, *1*) and, in the high-frequency area, the contribution of the mechanical generator is dominant (Fig. 5b, *4*).

The efficiency of the acoustic source of waves was assessed by recording the signals at the photo-receiver output for a fixed experimental geometry, constant amplitude of the modulating signal, and different values of frequency modulation in the range from 3 to 51 Hz with a step of 3 Hz. Under the assumption that the variation φ (the slope angle of the perturbed surface to the horizontal line) is small, the shift in the light ray on the photo receiver turns out to be prooutputional to φ and related to the output voltage V of the photo receiver as

$$\begin{gathered} u = V/V_{\max} = (\psi - \pi - \sin\psi)/\pi, \\ \psi = 2(\pi - \arccos(-\varphi L/a)). \end{gathered} \tag{1}$$

Here, a is the radius of the light spot on the photo receiver, L is the length of the ray from the reflection point to the plane of the photo receiver, $V_{\max}$ is the maximum voltage, and ψ is the intermediate angle function.

The solution to implicit equation (1) makes it possible to recover the dependence that angle φ has on the frequency based on the measured values of the voltage array V; the normalization to the maximum value determines the amplitude–frequency characteristics $\Phi(\omega)$ of the process of surface-wave generation. The values of $\Phi(f)$ (where $f = \omega/2\pi$)—calculated for two data arrays φ for $a = 0.15$ and $L = 12$ cm—are shown in Fig. 6 as solid and transparent circles.

The amplitude–frequency characteristics were theoretically estimated when analyzing the transformation of radiative pressure into the velocity of the acoustic flux and then into the amplitude of surface surface wave and slope of the wave surface at the point of measurement.

Because the surface surface wave is generated by the acoustic flux of the axisymmetric sound beam, the cross distribution of velocity $v(r, t)$ in a viscous liquid is given by the equation [12]

$$\frac{\partial v}{\partial t} - \frac{v}{r}\frac{\partial}{\partial r}\left(r\frac{\partial v}{\partial r}\right) = q(r, t), \tag{2}$$

where r is the distance to the beam axis, t is the time, ρ is the density, ν is the kinematic viscosity of the liquid, $q(r, t) = -\dfrac{\nabla P}{\rho}$, and ∇P is the gradient of radiative pressure. The Laplace transform with respect to the parameter s for Green's function of Eq. (2) [13]

$$G(r, t) = \frac{1}{4\pi\nu t}\exp\left(-\frac{r^2 + r_0^2}{4\nu t}\right)I_0\left(\frac{rr_0}{2\nu t}\right) \tag{3}$$

determines the transfer function of the transformation of radiative pressure into the velocity at point r [14]:

$$W_G(s, r) = \frac{1}{2\pi\nu} I_0(r_0\sqrt{s/\nu}) K_0(r\sqrt{s/\nu}) \tag{4}$$

and into the integral (with respect to the beam section) value of velocity v_a:

$$\begin{aligned} W_c(s) &= \int_0^R W_G 2\pi r dr \\ &= \int_0^R \frac{r}{\nu} I_0(r_0\sqrt{s/\nu}) K_0(r\sqrt{s/\nu}) dr. \end{aligned} \tag{5}$$

Here, r_0 is the radius for which the pressure gradient ∇P in the beam can be approximately assumed to be constant (see Fig. 3) and I_0 and K_0 are modified Bessel functions. In subsequent estimates, it is supposed that the elevation of the free surface by the acoustic beam has the form of a convex spherical segment with a height of ξ_0 and a root radius of R at the unperturbed surface.

The relation between the segment height ξ_0 and the acoustic flux velocity v follows from the balance of the kinetic energy of a unit mass of liquid $v_a^2/2$, gravity work, and surface tension:

$$\frac{v_a^2}{2} = g\frac{\xi_0}{2} + \gamma\frac{2\xi_0}{R^2} \text{ or } \frac{\xi_0}{v_a^2} = \frac{R^2}{gR^2 + 4\gamma}. \tag{6}$$

Here, g is the gravitational acceleration, σ is the coefficient of surface tension, and $\gamma = \sigma/\rho$.

The modulated acoustic beam generates ring waves with a frequency of ω, the amplitude of which is attenuated as going away from the point of intersection between the beam axis and surface. For deepwater conditions, the relation between the wave number k and frequency ω or phase velocity c of gravity–capillary wave is given by the dispersion relationship [14]

$$\omega^2 = gk + \gamma k^3 \text{ or } c^2 = g/k + \gamma k. \tag{7}$$

The spatial and temporal structure of the ring wave in deepwater conditions ($\lambda \ll H$) is prooutputional to $J_0(kr - \omega t)$ [15]. In view of source properties (6) and the geometric and viscous attenuation (prooutputional to $\exp(-\alpha t)$, where $\alpha = 2\nu k^2$ is the coefficient of viscous attenuation [16]), the ratio of the amplitude ξ_m of the surface ring wave entering the point r_c to the square of the velocity of acoustic flux in the source area is represented as

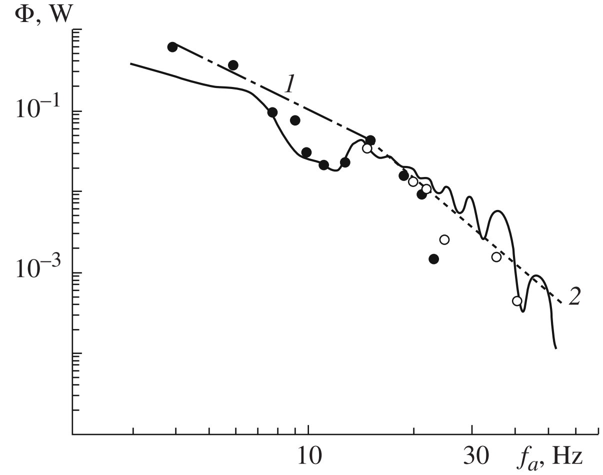

Fig. 6. Amplitude–frequency characteristics of the process of surface-wave generation by an acoustic beam: the solid line denotes the values calculated by formula (10), *1* and *2* are approximating functions, and the light and dark circles denote the experimental values.

$$W_\xi = \frac{\xi_m}{v_a^2} = \frac{R^2}{gR^2 + 4\gamma} \exp(-\alpha r_c/c) |J_0(kr_c)|. \tag{8}$$

Because the signal from the output of the laser-meter photo receiver is prooutputional to variations of the surface slope angle φ_m, which is related to the amplitude and wavelength by the approximate relation $\xi_m \approx \varphi_m\lambda/4 = \pi\varphi_m/2k$, expression (8) can be presented as a transfer function of the transformation of acoustic velocity into angle φ_m:

$$W_\varphi = \frac{\varphi_m}{v_a^2} = \frac{2}{\pi}\frac{k}{g + 4\gamma/R^2} \exp(-\alpha r_c/c) |J_0(kr_c)|. \tag{9}$$

Making the substitution $s = i\omega$ in (5), creating the quadratic form $W_s = W_c \times W_c^*$ (for converting v into v^2), and multiplying by (9), we obtain the through amplitude–frequency characteristic for the transformation of the variable $q(t) = -\frac{\nabla P}{\rho}$ into the angle of the surface-wave slope at the observation point r_c:

$$W(\omega) = W_s(\omega) \times W_\varphi(\omega). \tag{10}$$

The calculated values of $W(\omega)$ are shown as a solid line in Fig. 6 together with the points of the experimental amplitude–frequency characteristic Φ. The curve's form reflects the main features of the behavior of experimental points. The curves Φ and W are approximated by the power function $10 \times f^{-2}$ in the range of gravity waves ($f < 13$ Hz) and by the function

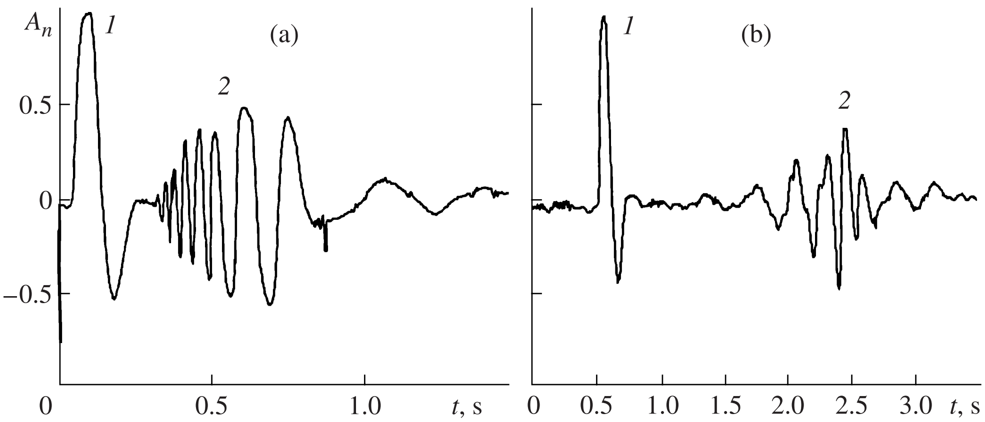

Fig. 7. Normalized perturbation values (A_n) near the boundary of (*1*) sound spot and (*2*) wave packets registered at a distance of (a) 10 cm and (b) 15 cm from the spot center.

$550 \times f^{-3.5}$ in the range of capillary waves ($f > 13$ Hz). The increase in the slope of the approximating functions with a growth in frequency is caused by the decreased efficiency of the acoustic flux and attenuated surface surface wave due to viscous attenuation. The local minimum in the neighborhood of the minimum of phase velocity of gravity–capillary waves (10–12 Hz) is caused by the reduced Q-factor of the system as a whole. In the high-frequency range ($f > 20$ Hz), the curve is characterized by oscillations caused by the multiplier $|J_0(kr_c)|$. The experimental points in this range of the spectrum are also characterized by considerable scattering; however, they are located near the curve.

The pattern of propagation of nonstationary surface waves generated upon the short-term influence of the acoustic beam was investigated in a series of experiments. Normalized to their proper maximum, the levels of signals from the specific electrical conductance sensor installed at the boundary of the sound spot (at a distance of 2 cm from its center) and from the laser meter of wave slopes are shown in Fig. 7. In these experiments, the duration of the acoustic pulse was 50 ms. At the boundary of sound spot, the electrical conductance sensor will register only an initial elevation and a compensating cavity (Fig. 7, curves *1*, represented in different time scales). At a short distance r_c, the signal has an expressed high-frequency component; at the observation point, a packet is registered with a frequency decreasing in time (Fig. 7a). This dispersion is typical for capillary waves, which attenuate relatively quickly with distance. At a distance of more than 15 cm, the main contribution to the signal is introduced by the gravity component; here, the signal oscillation frequency decreases with time (Fig. 7b).

To treat the wave packets with a quickly varying basic frequency, a wavelet analysis [17] is used, allowing us to obtain the arrival times of wave components of a given frequency. In calculations, the elementary functions were represented by biorthogonal wavelet pairs bior3.7 with a discretization interval $\Delta t = 0.001$ s. The field of representation of the initial signal (Fig. 8a) in the time–frequency coordinate system is shown in Fig. 8b. The density of darkening is prooutputional to the concentration of wavelets. The area of a maximum darkening marks the frequency of the wave arriving at a given time, which is calculated as $f = F_0/(\beta\Delta t)$, where F_0 is the central frequency of wavelet (0.9336 for bior3.7) and β is a scaling coefficient.

The curves of group velocity $cg = \dfrac{\partial\omega}{\partial k} = \dfrac{3c}{2} - \dfrac{g}{\omega}$ and phase velocity $c = \dfrac{\omega}{k}$, calculated in line with the theory of gravity–capillary waves in an ideal liquid, are shown as solid and dashed lines, respectively, in Fig. 9. The symbols denote the experimental wave propagation values registered at distances $r_c = 10$ and 15 cm away from the center of excitation area.

At a short distance ($r_c = 10$ cm), the packet consists mainly of capillary waves, the experimental points of which are located on the right (from the minimum) branch of the dispersion curve. When the distance increases to 15 cm, the high-frequency capillary waves attenuate almost completely and only the gravity waves marked in the left-side branch remain. The doubling of the sound intensity for the low distance $r_c = 10$ cm leads to an extension of the frequency range up to 45 Hz. For comparison, the data obtained for wave excitation by falling drops are also shown here. The frequency range of these waves goes up to 55 Hz; i.e., the drop-induced initial perturbation is shorter and of a wider range.

The velocities of waves excited by different methods are closely grouped near the theoretical curve of group velocity. The experimental results indicate that the phase characteristics of surface gravity–capillary

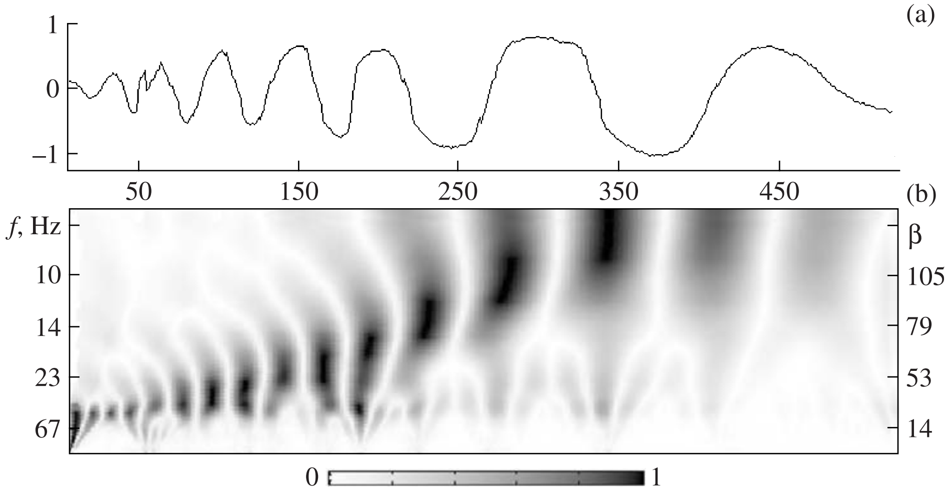

Fig. 8. (a) Graph of registered wave packets by the wave-slope sensor and (b) field of the amplitudes of the wavelet expansion components of the signal. The abscissa axis (time) is common for both. The left axis of ordinates is the incoming wave frequency *f*, and the right axis is the scaling coefficient β. The grayscale amplitudes are shown in the bottom.

waves excited by different sources agree satisfactorily with each other, and the time that the signal arrives at the measurement point is determined by the group velocity; i.e., $t_r = r_c/c_g$. The spectral analysis of the packets excited by acoustic pulses essentially depends on the propagation distance r_c.

CONCLUSIONS

The experimental results show that the acoustic beam falling normally onto the free surface serves as an efficient generator of surface waves in the gravity–capillary range. The given method makes it possible to relatively simply regulate the main wave parameters (frequency and amplitude) in the packet and continuous modes of generation.

Against the background of monotonic attenuation, the amplitude–frequency characteristic of the surface-wave generation process has a local dip near the minimum of phase velocity and growing oscillations in the high-frequency range.

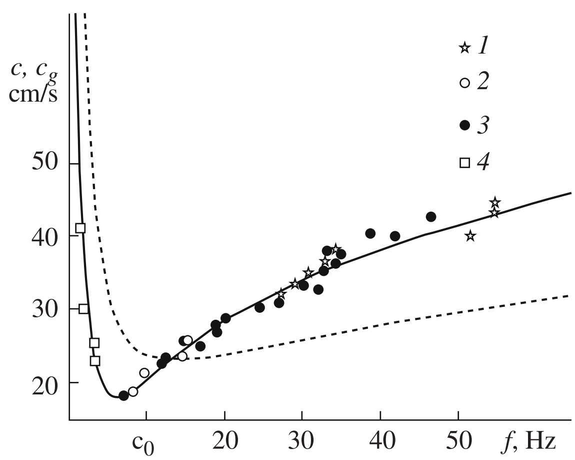

Fig. 9. The propagation velocity (c) of the wave components of nonstationary packets excited by sound pulses and falling water drops; the theoretical curve of the group velocity is denoted by c_g. The wave sources are as follows: (*1*) falling drop; (*2*) sound (nominal power), r_c = 10 cm; (*3*) sound (doubled power), r_c = 10 cm; and (*4*) sound (nominal power), r_c = 15 cm.

ACKNOWLEDGMENTS

The authors are grateful to I.V. Chernii, Dr. Phys.–Math. Sci., for bringing the problems of surface surface wave dynamics to our notice and for partial financial supoutput in upgrading the installation. This study was supported in part by the Division of Energetics, Mechanical Engineering, Mechanics, and Control Processes of the Russian Academy of Sciences, program OE-14 (Dynamics of multicomponent and heterogeneous liquids) and the Russian Foundation for Basic Research, project nos. 05-05-00473, 08-05-00473, and 08-05-90434.

REFERENCES

1. B. Kinsman, *Wind Waves* (Prentice-Hall, Englewood Cliffs, NJ, 1965).
2. V. Yu. Raizer and I. V. Chernyi, *Microwave Diagnostics of the Surface Layer of the Ocean* (Gidrometeoizdat, St. Petersburg, 1994) [in Russian].
3. A. M. Andreev and V. M. Ginzburg, “Refraction and Scattering of Electromagnetic Waves on Water-Air Surface, Deformed under the Action of Ultrasound Radiation Pressure,” Radiotekh. Elektron. (Moscow) **30**, 881–885 (1985).

4. M. W. Dingemans, *Water Wave Propagation Over Uneven Bottoms. Pt. 1. Linear Wave Propagation. Pt. 2. Non-Linear Wave Propagation. Advanced Series on Ocean Engineering. V. 13: Hydraulics* (World Sci., Singapore, The Netherlands, 1997).
5. A. V. Kistovich and Yu. D. Chashechkin, "Dynamics of Gravity-Capillary Waves on the Surface of a Nonuniformly Heated Fluid," Izv. Akad. Nauk, Fiz. Atmos. Okeana **43**, 109–116 (2007) [Izv., Acad. Sci., Atmos. Oceanic Phys. **43**, 95 (2007)].
6. A. V. Dolgikh, D. L. Dorofeev, and B. A. Zon, "Capillare Waves of Finite Amplitude with Tolmen Nonlinearity," Izv. RAN, Mekh. Zhidk. Gaza, No. 2, 148–153 (2007).
7. E. I. Parau, J. Vanden-Broeck, and M. J. Cooker, "Nonlinear Three-Dimensional Gravity-Capillary Solitary Waves," J. Fluid Mech. **536**, 99–105 (2005).
8. T. H. C. Herbers, S. Elgar, N. A. Sarap, and R. T. Guza, "Nonlinear Dispersion of Surface Gravity Waves in Shallow Water," J. Phys. Oceanogr. **32**, 1181–1192 (2002).
9. Yu. A. Volkov, A. V. Kuz'min, A. P. Medvedev, et al., "Radiometric Studies of the Water-Surface Temperature Regime under Laboratory Conditions," Izv. Akad. Nauk, Fiz. Atmos. Okeana **40**, 96–101 (2004) [Izv., Acad. Sci., Atmos. Oceanic Phys. **40**, 86 (2004)].
10. F. Zhu, R. Miao, C. Xu, and Z. Cao, "Measurement of the Dispersion Relation of Capillary Waves by Laser Diffraction," Amer. J. Phys. **75**, 896–898 (2007).
11. V. A. Shutilov, *Fundamental Physics of Ultrasound* (Leningr. Gos. Univ., Leningrad, 1980) [in Russian].
12. V. Ya. Arsenin, *Methods of Mathematical Physics and Special Functions* (Nauka, Moscow, 1974) [in Russian].
13. H. Carslaw and D. Eger, *Operational Methods in Applied Mathematics* (Dover, New York, 2000; Inostr. Liter., Moscow, 1948).
14. N. E. Kochin, N. A. Kibel', and N. V. Roze, *Theoretical Hydromechanics* (Fizmatgiz, Moscow, 1963; Wiley Intersci., New York, 1964), Part 1.
15. N. S. Koshlyakov, E. B. Gliner, and M. M. Smirnov, *Differential Equations of Mathematical Physics* (Vyssh. Shkola, Moscow, 1970) [in Russian].
16. L. D. Landau and E. M. Lifshitz, *Fluid Mechanics*, 2nd ed. (Nauka, Moscow, 1986; Pergamon Press, Oxford, 1987).
17. A. A. Koronovskii and A. E. Khramov, *Continuous Wavelet Analysis and its Applications* (Fizmatlit, Moscow, 2003) [in Russian].